

# Controlled synthesis of core–shell iron–silica nanoparticles and their magneto-dielectric properties in polymer composites

T I Yang<sup>1</sup>, R N C Brown<sup>2</sup>, L C Kempel<sup>3</sup> and P Kofinas<sup>1</sup>

<sup>1</sup> Fischell Department of Bioengineering, University of Maryland, College Park, MD 20742, USA

<sup>2</sup> Department of Chemical and Biomolecular Engineering, University of Maryland, College Park, MD 20742, USA

<sup>3</sup> Department of Electrical and Computer Engineering, Michigan State University, East Lansing, MI 48824, USA

E-mail: [kofinas@umd.edu](mailto:kofinas@umd.edu)

Received 5 November 2010, in final form 20 December 2010

Published 2 February 2011

Online at [stacks.iop.org/Nano/22/105601](http://stacks.iop.org/Nano/22/105601)

## Abstract

Low loss core–shell iron–silica nanocomposites with improved magneto-dielectric properties at radio frequencies (1 MHz–1 GHz) were successfully fabricated. A new simple method was developed to synthesize metallic iron (Fe) nanoparticles with uniform size distribution in an aqueous environment at room temperature. Citric acid and oleic acid served as surface-capping agents to control the particle size of the synthesized Fe nanoparticles. Smaller Fe nanoparticles with narrower particle size distribution were obtained as the concentration ratio of iron ions to carboxylic acid groups decreased. The Fe nanoparticles were subsequently coated with silica (SiO<sub>2</sub>) layers to prevent the iron cores oxidizing. Polymer composites were prepared by incorporating Fe@SiO<sub>2</sub> nanoparticles with polydimethylsiloxane (PDMS) elastomers. Experimental results showed that the dielectric permittivity ( $\epsilon$ ) and magnetic permeability ( $\mu$ ) of the polymer composite increased with increasing amount of Fe@SiO<sub>2</sub> nanoparticle doping. The dielectric loss ( $\tan \delta$ ) was near 0.020 at a frequency of 1 GHz.

## 1. Introduction

Materials having high values of magnetic permeability ( $\mu$ ) and dielectric permittivity ( $\epsilon$ ) are promising for advanced applications in microwave communication devices and their miniaturization. Polymer-based composites are preferred because of their light weight, shape-flexibility and better processability. However, ferrimagnetic resonance restricts the use of conventional ferrite–polymer composites to frequencies much lower than 1 GHz since there is no appreciable magnetic permeability ( $\mu$ ) beyond the resonance frequency ( $f_{\text{res}}$ ). For example, MnZn and NiZn ferrites are only suitable for use up to 2 MHz and 200 MHz, respectively [1]. Furthermore, the Snoek limit predicts that the product of  $\mu$  and  $f_{\text{res}}$  is limited by the saturation magnetization ( $M_s$ ) [2, 3].

Therefore, high  $\mu$  at high operational frequency cannot be expected from ferrites due to their intrinsically low saturation magnetization ( $M_s$ ). Ferromagnetic iron (Fe) is an ideal candidate for high  $\mu$  composites due to its high magnetic permeability and saturation magnetization at room temperature (218 emu g<sup>-1</sup>) [4]. However, the eddy current arising from its high electrical conductivity causes energy loss at microwave frequencies. The adverse effect of eddy current could be suppressed by utilizing iron particles with a size below the so-called ‘skin depth’, which is typically near 1  $\mu\text{m}$  at microwave frequencies [5, 6].

Fe nanoparticles (less than 1  $\mu\text{m}$ ) with uniform particle size distribution are only accessible by high temperature thermolysis in oil-based reaction systems [7–10]. However, these reactions are considered as hazardous processes because

of the involvement of non-stable and toxic reagents, the potential for explosion, and the high energy consumption. In addition, the synthesized Fe nanoparticles immediately oxidize upon exposure to air if there is no protection on the Fe particle surface. We report a simple synthesis method in which the reaction is conducted in aqueous environments and at room temperature, resulting in Fe nanoparticles with a uniform size distribution. The Fe particle size is controllable using surface-capping agents (oleic acid and citric acid). The Fe nanoparticles are subsequently coated with silica (SiO<sub>2</sub>) layers to prevent oxidation of the iron cores [11, 12]. A novel polymer composite with high permeability ( $\mu$ ) and low energy loss was prepared using such core-shell Fe@SiO<sub>2</sub> nanoparticles in polydimethylsiloxane (PDMS) matrices. The SiO<sub>2</sub> shells provide electrically insulating layers which decrease energy loss ( $\tan \delta$ ) and additionally prevent the possibility of  $\mu$  decrease due to Fe oxidation. Furthermore, the SiO<sub>2</sub> layers also improve the compatibility of core-shell Fe@SiO<sub>2</sub> particles with PDMS polymer matrices due to the similar nature of chemical bonds (Si–O–Si) [13]. The morphology of the magnetic nanocomposites was characterized by transmission electron microscopy (TEM). The magneto-dielectric properties of the polymer particle composites in the mega-to giga-frequency range were evaluated using an impedance analyzer.

## 2. Experimental section

### 2.1. Materials

Iron chloride (FeCl<sub>3</sub>, 97%), oleic acid (90%), tetraethyl orthosilicate (TEOS; 99.99%), (3-aminopropyl)trimethoxysilane (APS; 97%) palladium(II) chloride (PdCl<sub>2</sub>, 99%), sodium borohydride (NaBH<sub>4</sub>; 98%), and citric acid monohydrate (98%) were purchased from Sigma-Aldrich. Deionized water was obtained using a Milli-Q water purification system (Millipore, Billerica, MA, USA). The liquid components (Sylgard 184) of PDMS were supplied by Dow Corning Corporation. All chemicals were used as-received.

### 2.2. Iron (Fe) nanoparticle synthesis

Fe nanoparticles were synthesized at room temperature from FeCl<sub>3</sub> using NaBH<sub>4</sub> as a reducing agent and PdCl<sub>2</sub> which serves as a nucleating agent. The concentration ratio ( $R_{+/-}$ ) of iron ions (Fe<sup>3+</sup>) to oleic acid (OA) and citric acid monohydrate (CA) was systematically varied and its effect on the resulting nanoparticle size was studied. The concentration ratio ( $R_{+/-}$ ) is defined as the ratio of total positive (Fe<sup>3+</sup>) to negative charges (CA and OA) which can be present in solution. The  $R_{+/-}$  is calculated to be  $3[\text{Fe}^{3+}]/([\text{OA}] + 3[\text{CA}])$ . In a typical nanoparticle synthesis procedure ( $R_{+/-} = 0.86$ ), 0.16 mmol FeCl<sub>3</sub>, 0.16 mmol CA, 0.08 mmol OA and 0.1 ml PdCl<sub>2</sub> solution (0.01 M) were dissolved in a mixed solvent (150 ml water and 40 ml ethanol). After purging with a gas mixture [95% argon (Ar) and 5% hydrogen (H<sub>2</sub>)] for 30 min, 0.06 g NaBH<sub>4</sub> of 10 ml water solution was added in one shot. The mixture immediately became black, indicating the formation of Fe nanoparticles.

### 2.3. Silica (SiO<sub>2</sub>) shell formation on iron (Fe) nanoparticle cores

Following Fe nanoparticle formation, the solution was kept stirred for 20 min to ensure the completion of the redox reaction. 14  $\mu$ l APS and 169  $\mu$ l TEOS were added into the solution to coat the Fe nanoparticles with SiO<sub>2</sub> layers [14]. The reaction was allowed to proceed for 3 h with Ar/H<sub>2</sub> gas purging before magnetically collecting the core-shell nanoparticles. The nanoparticles were washed with ethanol to remove any residue.

### 2.4. Preparation of Fe@SiO<sub>2</sub> nanocomposites

The Fe@SiO<sub>2</sub>/polymer nanocomposites were prepared by incorporating Fe@SiO<sub>2</sub> core-shell nanoparticles into PDMS elastomers. In a typical formulation, 1 g of liquid components of PDMS elastomers was mixed with the desired amount of Fe@SiO<sub>2</sub> core-shell nanoparticles (0.54 g for a 35 wt% composite) to obtain a homogeneous solution. The solution was subsequently poured into a mold and cured at 70 °C overnight, resulting in a flexible polymer nanoparticle composite.

### 2.5. Characterization

TEM (JEOL 200CX) was used to observe the morphology of the nanoparticles. The particle size is reported as the average observed size ( $D_{\text{avg}}$ ), which is the average particle size of approximately 1000 individual particles from multiple TEM images. Magnetic properties were investigated using a vibrating sample magnetometer (VSM; Lakeshore 7400 series). The powder x-ray diffraction measurements (XRD) of the samples were obtained on a Bruker C2 Discover and D8 Advance systems using Cu K $\alpha$  ( $\lambda = 0.154$  nm) radiation. The crystallite size ( $D_{\text{XRD}}$ ) of the synthesized nanoparticles was measured using the Scherrer formula [15]:

$$D_{\text{XRD}} = \frac{0.94\lambda}{B \cos \theta} \quad (1)$$

where  $\lambda$  is the x-ray wavelength, the width  $B$  is measured at an intensity equal to half the maximum intensity, and  $\theta$  is the Bragg angle.

X-ray photoelectron spectroscopy (XPS, Kratos AXIS 165) was used to investigate the oxidation state of iron. The charge-shifted spectra were corrected assuming that the adventitious C 1s peak detected was at 284.600 eV. Energy dispersive x-ray spectroscopy (EDS) equipped within the TEM was used to determine the chemical composition of the synthesized nanoparticles. The magneto-dielectric properties (relative dielectric permittivity,  $\epsilon_r$ , and relative magnetic permeability,  $\mu_r$ ) in the 1 MHz–1 GHz range were measured using an Agilent RF impedance/material analyzer (E4991A). Samples for  $\epsilon_r$  measurement were prepared in the shape of a solid disc with a diameter of 0.75 in and a thickness of 0.1 in. Samples for  $\mu_r$  measurement were in the geometry of a washer with an outer diameter of 0.75 in, an empty inner diameter of 0.25 in, and a thickness of 0.1 in. Multiple measurements (five times) were obtained and their standard deviations were calculated.

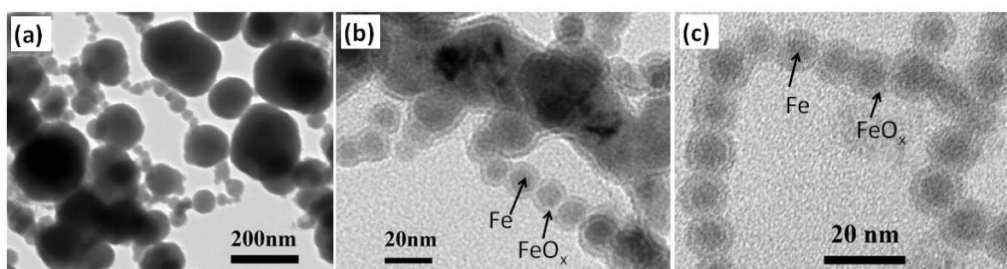


**Figure 1.** TEM images of Fe nanoparticles synthesized at various concentration ratios ( $R_{+/-}$ ) of  $\text{Fe}^{3+}$  to citric acid: (a)  $R_{+/-} = 10$ ; (b)  $R_{+/-} = 1$ ; (c)  $R_{+/-} = 0.7$ . Pictures show oxide layers ( $\text{FeO}_x$ ) formed after exposing particles to air during sample preparation.

### 3. Results and discussion

#### 3.1. Fe nanoparticle synthesis (assisted by citric acid)

Citric acid (CA) has been traditionally utilized as a surface-capping agent to control the formation of metallic nanoparticles such as cobalt [14], gold [16], palladium [17], and silver [18]. In our Fe nanoparticle synthesis we also utilize  $\text{PdCl}_2$ , which serves as a nucleating agent, along with CA to control Fe nanoparticle formation. After reduction by a reducing agent ( $\text{NaBH}_4$ ),  $\text{Pd}^{2+}$  ions became metallic Pd seeds for heterogeneous nucleation and growth of Fe nanoparticles [19].

Figure 1(a) shows that the Fe particle size ranges from 200 to 20 nm as the concentration ratios ( $R_{+/-}$ ) of  $\text{Fe}^{3+}$  to CA remained at 10. This result indicated that the amount of CA cannot control Fe nanoparticle formation when there are more  $\text{Fe}^{3+}$  than CA present in the solution. A larger number of particles with narrow size distribution (11–15 nm) combined with few irregular large particles was obtained when increasing the amount of CA ( $R_{+/-} = 1$ ), as shown in figure 1(b). When the amount of CA was increased and  $R_{+/-}$  became 0.7, uniform Fe nanoparticles with an average size of 11 nm were successfully synthesized (figure 1(c)). These results suggest that a greater amount of CA (or lower  $R_{+/-}$ ) leads to smaller particles with more uniform size distribution, which is consistent with other reports [14, 17, 18]. The carboxylic acid groups ( $\text{COO}^-$ ) of CA can effectively associate with  $\text{Fe}^{3+}$  to control the concentration of free  $\text{Fe}^{3+}$  ions in solution. Therefore it is easier to control Fe nanoparticle formation when there are more  $\text{COO}^-$  than  $\text{Fe}^{3+}$  ions present in solution ( $R_{+/-} < 1$ ). However, CA is a strong chelating agent for iron, meaning that it has the ability to dissolve Fe particles into iron-citrate-complexes [20]. Our results shows that the synthesized Fe nanoparticles re-dissolved into solution within 30 min of particle formation for values of  $R_{+/-}$  below 1. Therefore, it is not feasible to use CA alone to obtain Fe nanoparticles with a uniform size distribution.

#### 3.2. Fe nanoparticle synthesis (assisted by oleic acid)

OA surfactant is a well-known surface-capping agent for its ability to control nanoparticle formation. There have been numerous literature reports on obtaining magnetic nanoparticles with uniform particle size distribution with the assistance of OA in synthetic processes [21]. In our Fe

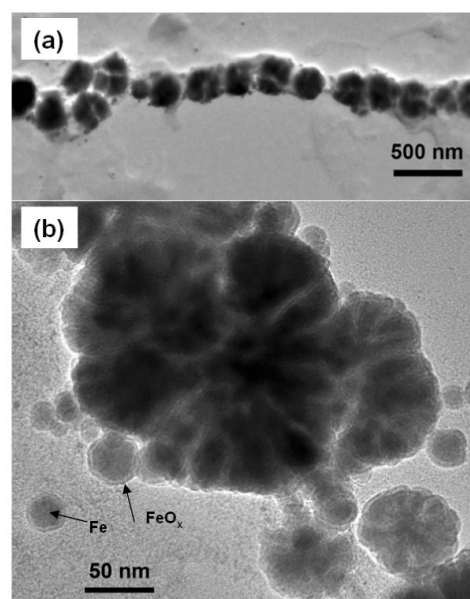


**Figure 2.** TEM images of Fe nanoparticles synthesized at a concentration ratio of  $\text{Fe}^{3+}$  to oleic acid equal to 1: (a) low magnification; (b) high magnification. Pictures show oxide layers ( $\text{FeO}_x$ ) formed after exposing particles to air during sample preparation.

synthesis, the resulting particles (10–30 nm) aggregated and formed clusters when the concentration ratio  $R_{+/-}$  of  $\text{Fe}^{3+}$  to OA was equal to 1 (figure 2). Furthermore, increasing the amount of OA (or  $\text{COOH}$ ) did not result in good control of Fe nanoparticle formation. Instead, no Fe nanoparticles formed for  $R_{+/-}$  of 0.75 and 0.85. This result indicated that OA was also not an effective way to control nanoparticle formation.

#### 3.3. Fe nanoparticle synthesis (assisted by CA and OA)

Both CA and OA were used to control Fe nanoparticle formation to avoid re-dissolution due to excess CA. The concentration ratio of CA to OA used in the synthesis was kept at 2. Figure 3(a) shows that Fe nanoparticles with an observed average size  $D_{\text{avg}}$  of  $16.6 \pm 4.5$  nm could be successfully synthesized at  $R_{+/-} = 1.7$ . However, the poor particle size distribution ( $\pm 4.5$  nm) of these larger particles suggests that the particle formation was not controlled. For this reason, the concentration of carboxylic acid [ $\text{COO}^-$ ] groups was

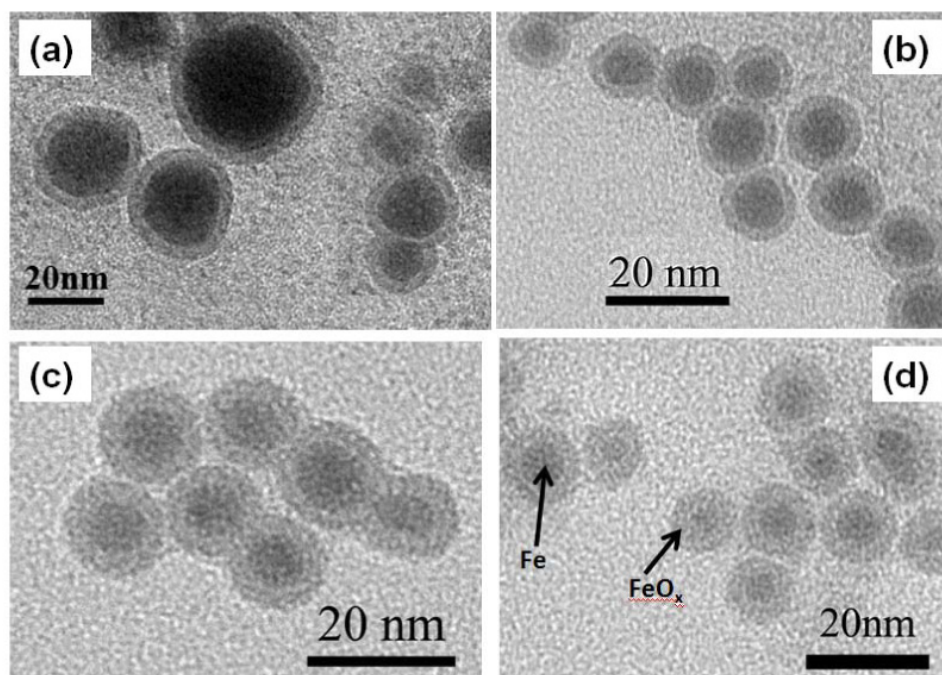


**Figure 3.** TEM images of Fe nanoparticles synthesized at various concentration ratios ( $R_{+/-}$ ) of  $\text{Fe}^{3+}$  to citric acid and oleic acid: (a)  $R_{+/-} = 1.7$ ; (b)  $R_{+/-} = 0.86$ ; (c)  $R_{+/-} = 0.75$ ; (d)  $R_{+/-} = 0.5$ . Pictures show oxide layers ( $\text{FeO}_x$ ) formed after exposing particles to air during sample preparation.

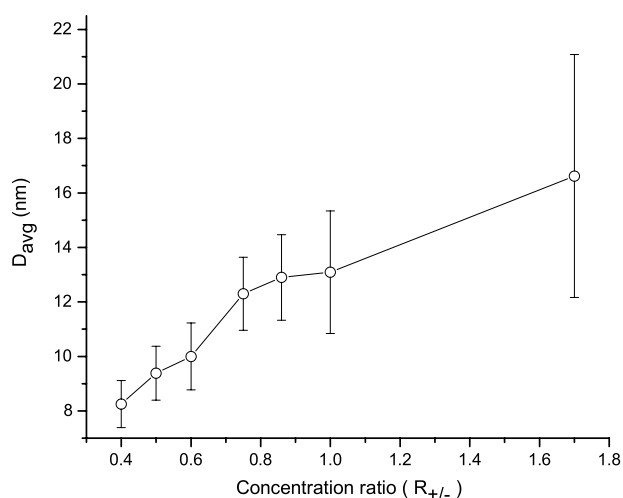


**Figure 4.** Effect of concentration ratio ( $R_{+/-}$ ) on Fe nanoparticle size distribution.

increased (decreasing  $R_{+/-}$ ) to narrow the particle distribution. The results show that Fe nanoparticles with uniform particle distribution could be obtained with decreasing  $R_{+/-}$  (figure 3). For example, the resulting  $D_{\text{avg}}$  was  $12.9 \pm 1.6$  nm and  $9.4 \pm 1.0$  nm as  $R_{+/-}$  decreased from 0.86 to 0.5, respectively. The narrow size distribution contributes to optimum  $\text{COO}^-$  group concentration and Pd seeding. The  $\text{COO}^-$  groups can effectively associate with  $\text{Fe}^{3+}$  to prevent the free  $\text{Fe}^{3+}$  ions in solution from nucleating and also to slowly release  $\text{Fe}^{3+}$  ions to Pd seed surfaces to grow, thus leading to uniform Fe nanoparticles. In summary, Fe nanoparticle formation could be controlled when using both CA and OA together as surface-

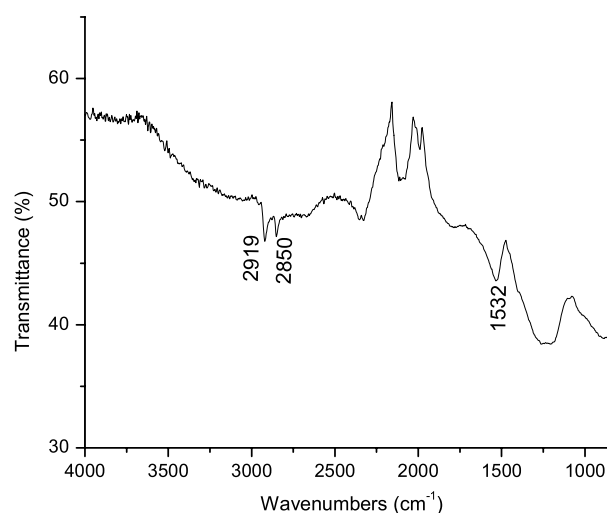


**Figure 5.** FTIR spectroscopy spectrum of synthesized Fe nanoparticles.

capping agents. Fe nanoparticles with sizes varying from  $16.6 \pm 4.5$  nm to  $8.2 \pm 0.8$  nm could be obtained as  $R_{+/-}$  decreased from 1.7 to 0.4. Higher  $[\text{COO}^-]$  (or lower  $R_{+/-}$ ) led to smaller Fe nanoparticles with narrower size distribution as summarized in figure 4. Moreover, there is no indication of re-dissolution of Fe in spite of the high concentration of  $[\text{COO}^-]$  present in solution ( $R_{+/-} = 0.4$ ).

**Chemical structure.** Fourier transform infrared spectroscopy (FTIR) confirmed that the surface of synthesized nanoparticles was coated with surface-capping agents (CA and OA), as shown in figure 5. The broad peak between 3500 and

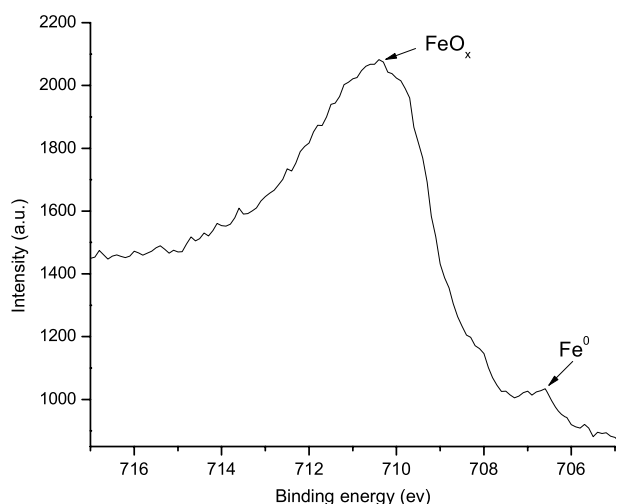


**Figure 6.** XPS spectrum of synthesized Fe nanoparticles. The  $\text{FeO}_x$  peak is due to exposure of particles to air during the XPS experiment.

$2500\text{ cm}^{-1}$  is attributed to the O–H stretch of the  $\text{COO}^-$  groups from the surface-capping agents. Two sharp bands at  $2919$  and  $2850\text{ cm}^{-1}$  are attributed to the asymmetric  $\text{CH}_2$  stretch and the symmetric  $\text{CH}_2$  stretch from OA, respectively. The broad peak near  $1200\text{ cm}^{-1}$  is due to CO stretching or OH deformation from the surface-capping agents. The bands at  $1532\text{ cm}^{-1}$  are characteristic of  $\text{COO}^-$  stretch, which confirm that OA was chemisorbed as a carboxylate onto the nanoparticle surface, consistent with what has been reported in literature [22].

High-resolution XPS was utilized to determine the oxidation state of the nanoparticles, and is shown in figure 6. The binding energy of Fe  $2p_{3/2}$  ( $706.7\text{ eV}$ ) confirms that the synthesized nanoparticles were metallic  $\text{Fe}^0$  [23]. In addition, the binding energy at  $710.3\text{ eV}$  indicated the formation of iron oxides ( $\text{FeO}_x$ ,  $x = 1\text{--}1.5$ ) due to exposure to air. EDS revealed the chemical composition of synthesized nanoparticles, as shown in figure 7. No contaminating elements from reagents, such as boron, sodium, or chlorine, except palladium, were detected (note: the copper and carbon signals were from the TEM grid used in the EDS measurement). The palladium was from the catalyst ( $\text{PdCl}_2$ ) used to promote the redox reaction. The ratios of  $[\text{Pd}^{2+}]$  to  $[\text{Fe}^{3+}]$  in the synthesis were varied between 0.01 to 0.003 at the values of  $R_{+/-}$  varied between 0.5 and 1.7. EDS data revealed that the nanoparticles synthesized for all  $R_{+/-}$  values comprised Fe ( $>99\%$ ) and Pd ( $<1\%$ ). In summary, the nanoparticles synthesized in this study are metallic  $\text{Fe}^0$  ( $>99\%$ ) coated with both CA and OA.

### 3.4. Iron (Fe)@silica ( $\text{SiO}_2$ ) core-shell nanoparticles

The synthesized Fe nanoparticles were coated with silica ( $\text{SiO}_2$ ) via a sol-gel reaction [14]. For application in microwave communication devices, the  $\text{SiO}_2$  shells provide electrical insulating layers which decrease energy loss ( $\tan\delta$ ) and additionally prevent the possibility of  $\mu$  decrease due to Fe oxidation. Figure 8 shows that the  $12.9 \pm 1.6\text{ nm}$  Fe nanoparticles ( $R_{+/-} = 0.86$ ) were successfully coated with

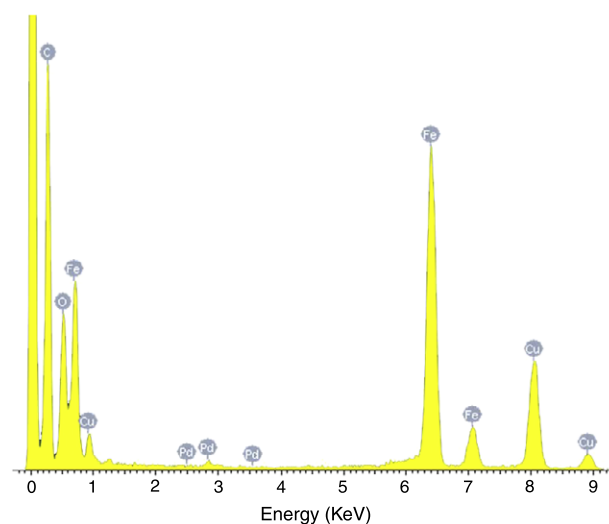


**Figure 7.** EDS spectrum of synthesized Fe nanoparticles. (This figure is in colour only in the electronic version)

$2\text{ nm SiO}_2$  layers with no signs of any Fe oxidation ( $\text{FeO}_x$ ). The chain-like assemblies of Fe nanoparticles were due to strong magnetic dipole-dipole interaction between individual Fe nanoparticles which were subsequently fixed by the  $\text{SiO}_2$  layers during the hydrolysis reaction. This phenomenon of chain-like nanoparticle formation has also been reported in cobalt and nickel systems [24, 25].

However, the Fe core in the synthesized  $\text{Fe@SiO}_2$  nanoparticles gradually oxidized and formed a thin layer of  $\text{FeO}_x$ , as shown in figure 9(a). The Fe oxidation indicated that the  $\text{SiO}_2$  protection layers were not dense enough to prevent oxygen from permeating the  $\text{SiO}_2$  layers and oxidizing the Fe cores. In addition, there is no distinct diffraction pattern from the synthesized nanoparticles of figure 9(b), indicating the amorphous nature of the  $\text{Fe@SiO}_2$  nanoparticles. The synthesized  $\text{Fe@SiO}_2$  nanoparticles were hence heat-treated at  $400^\circ\text{C}$  under an  $\text{Ar}/\text{H}_2$  atmosphere for 1 h to improve their crystalline structure and to densify the  $\text{SiO}_2$  layers [26].

Figure 10(a) shows that the Fe nanoparticles began to sinter together after heat-treatment. The structural information was obtained from both TEM selected area electron diffraction (SAED) and wide angle XRD. Figure 10(b) depicts a SAED pattern from the heat-treated  $\text{Fe@SiO}_2$  nanoparticles, showing multiple diffraction rings. The calculated lattice d-spacings derived from the diffraction rings are  $2.00$  (ring 1),  $1.44$  (ring 2),  $1.17$  (ring 3), and  $1.02$  (ring 4)  $\text{\AA}$ , corresponding to the (110), (200), (211), and (220) planes of  $\alpha\text{-Fe}$ , respectively [27]. Figure 11 shows the XRD patterns of heat-treated  $\text{Fe@SiO}_2$  nanoparticles. The positions of all diffraction rings/peaks are consistent with standard  $\alpha\text{-Fe}$  powder diffraction data reported in literature [27] and no other iron oxides ( $\text{FeO}_x$ ) could be identified. Furthermore, no obvious iron oxide layers  $\text{FeO}_x$  were observed after 6 months, indicating the  $\text{SiO}_2$  already functioned as a protection layer to prevent Fe cores from oxidation. In addition to the crystalline structure, the crystallite size of synthesized Fe nanoparticles could be obtained from their XRD peaks using Scherrer's formula. The calculated

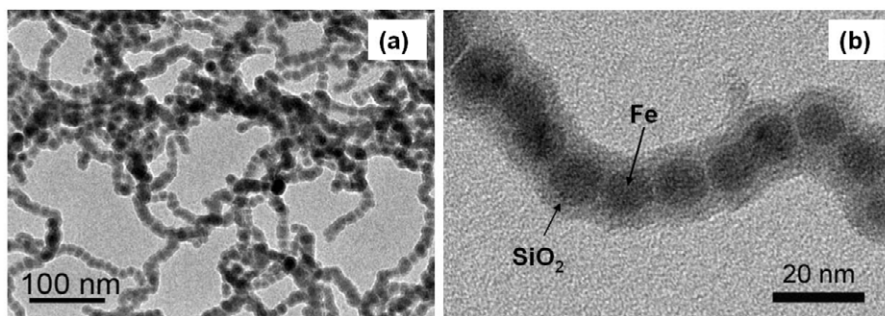


**Figure 8.** TEM image of Fe@SiO<sub>2</sub> nanoparticles: (a) low magnification; (b) high magnification.

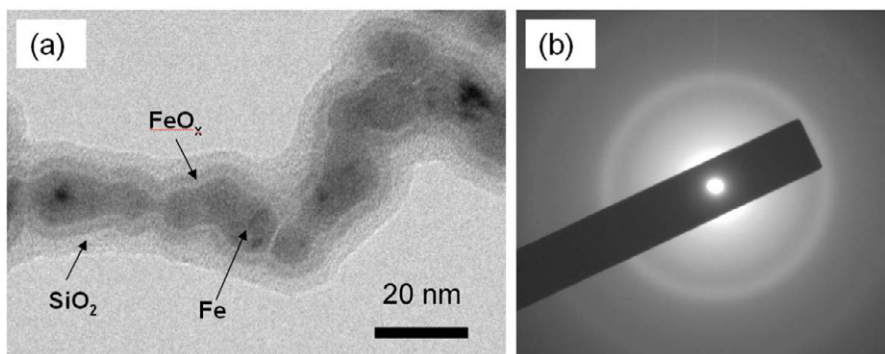


**Figure 9.** (a) TEM image of Fe@SiO<sub>2</sub> nanoparticles without heat-treatment; (b) selected area electron diffraction pattern of nanoparticles.

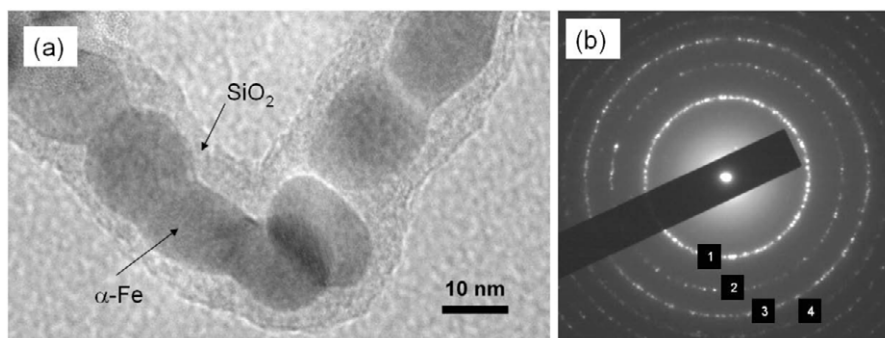


**Figure 10.** (a) TEM image of Fe@SiO<sub>2</sub> nanoparticles with heat-treatment; (b) selected area electron diffraction pattern of nanoparticles.

average crystallite size ( $D_{\text{XRD}}$ ) is 10 nm, which is close to the size observed ( $12.9 \pm 1.6$  nm) by TEM, indicating that the synthesized Fe nanoparticles did not coalesce into larger crystallites after heat-treatment.

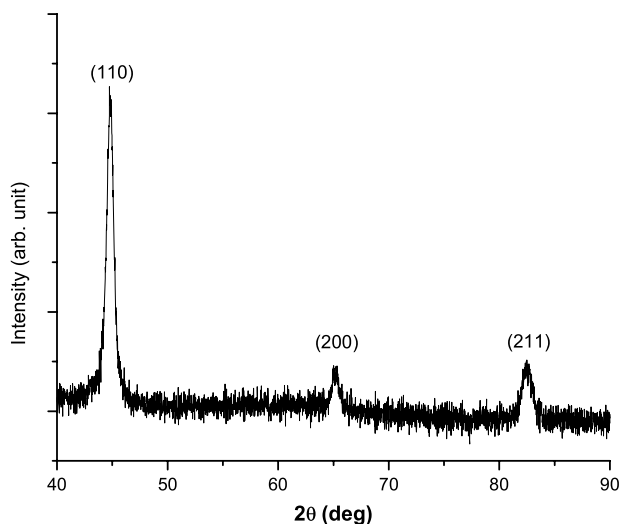
### 3.5. Magnetic properties of Fe@SiO<sub>2</sub> nanoparticles

Figure 12 shows the room temperature magnetization as a function of applied magnetic field for  $12.9 \pm 1.6$  nm Fe@SiO<sub>2</sub> nanoparticles ( $R_{+/-} = 0.86$ ). For the particles without heat-treatment, there is hysteresis present with a coercivity ( $H_c$ ) of 800 Oe and a saturation magnetization ( $M_s$ ) of  $52 \text{ emu g}^{-1}$ , which is consistent with ferromagnetic behavior. It has been reported in literature that the Fe critical size ( $D_{\text{SP}}$ ) for superparamagnetic to ferromagnetic transition is close to 10 nm [4]. Therefore, the  $12.9 \pm 1.6$  nm Fe@SiO<sub>2</sub>

nanoparticles should be ferromagnetic [4]. Moreover, the heat-treated Fe@SiO<sub>2</sub> nanoparticles show ferromagnetic behavior with higher values of  $H_c$  (1200 Oe) and  $M_s$  ( $100 \text{ emu g}^{-1}$ ) compared to particles without heat-treatment. This indicated that the heat-treatment improved the purity (due to removal of FeO<sub>x</sub>, surface-capping agents, etc) and the crystalline structure of Fe cores in the Fe@SiO<sub>2</sub> nanoparticles, leading to improved magnetic properties: higher values of  $H_c$  and  $M_s$  for Fe@SiO<sub>2</sub> particles.

### 3.6. Magneto-dielectric properties of the Fe@SiO<sub>2</sub>/polymer composites

The size of the synthesized Fe@SiO<sub>2</sub> particle is crucial for obtaining Fe@SiO<sub>2</sub>/PDMS composites with improved magneto-dielectric properties (magnetic permeability,  $\mu$ , and



**Figure 11.** Wide angle x-ray diffraction pattern of synthesized Fe@SiO<sub>2</sub> nanoparticles.

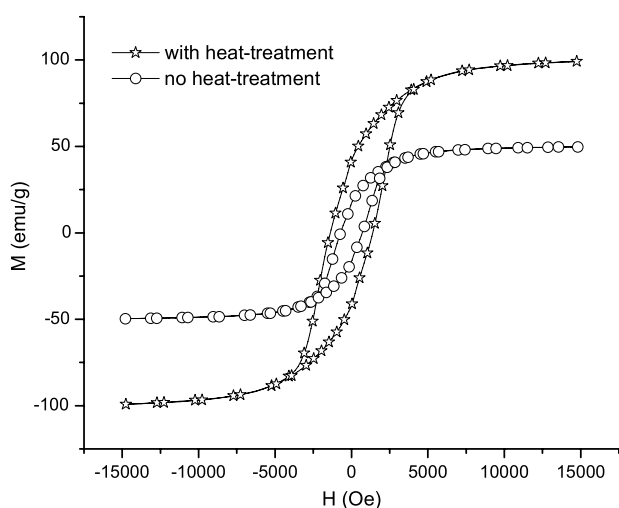


**Figure 12.** Magnetization ( $M$ ) versus applied magnetic field ( $H$ ) for Fe@SiO<sub>2</sub> nanoparticles at 300 K.

dielectric permittivity,  $\epsilon$ ). It has been reported in the literature that polymer nanocomposites with single domain ferromagnetic nanoparticles could have optimal magnetic permeability ( $\mu$ ) [28, 29]. For the particles with magnetic multi-domains, the magnetic permeability of the polymer composite is low due to particle magnetic domain wall movement. More domain wall movement results in a lower ability to respond to the applied magnetic alternating field, thus leading to lower magnetization and magnetic permeability. For magnetic nanoparticles in the superparamagnetic state, the anisotropy energy sustaining the particle's magnetization becomes comparable to the thermal energy from the magnetic nanoparticles' surroundings. Therefore, thermal energy effects cause significant fluctuations in nanoparticle magnetic moments and reduces their resultant magnetization and permeability. For iron particles the optimum size range to obtain high  $\mu$  is between 10 and 17 nm, where single domain ferromagnetic particles without any domain

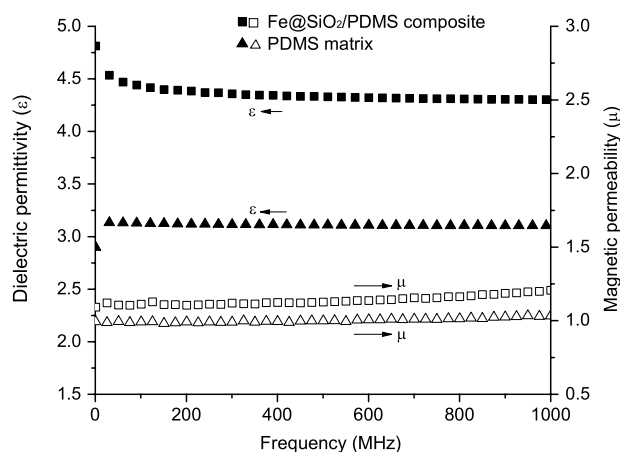


**Figure 13.** Dielectric permittivity,  $\epsilon$ , (closed symbol) and magnetic permeability,  $\mu$ , (open symbol) of Fe@SiO<sub>2</sub>/PDMS composites.

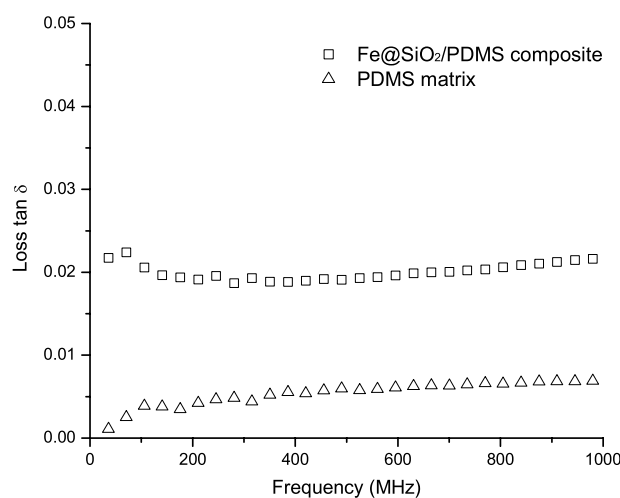


**Figure 14.** Dielectric loss  $\tan \delta$  of Fe@SiO<sub>2</sub>/PDMS composites.

walls are present [30]. For this reason,  $12.9 \pm 1.6$  nm Fe@SiO<sub>2</sub> nanoparticles ( $R_{+/-} = 0.86$ ) were chosen to prepare polymer composites. The Fe@SiO<sub>2</sub>/polymer nanocomposites were prepared by incorporating Fe@SiO<sub>2</sub> core-shell nanoparticles with PDMS elastomers. The resulting dielectric permittivity ( $\epsilon$ ) and magnetic permeability ( $\mu$ ) of the polymer nanocomposites are shown in figure 13. The dielectric permittivity of the PDMS matrix ( $\epsilon = 3.1$ ) improved from 3.1 to 4.3 at 1 GHz with 35% Fe@SiO<sub>2</sub> nanoparticle doping. The magnetic permeability of the PDMS matrix ( $\mu = 1$ ) also improved from 1.0 to 1.2 at 1 GHz with doping with 35% Fe@SiO<sub>2</sub> nanoparticles. The dielectric loss  $\tan \delta$  was less than 0.020 at the 1 GHz frequency range, as shown in figure 14. The dielectric response of the nanoparticle composites at applied alternating field is described in terms of the complex permittivity ( $\epsilon^*$ ) which is represented by its real and imaginary parts.

$$\epsilon^* = \epsilon' - i\epsilon'' \quad (2)$$

where  $\epsilon'$  is the dielectric permittivity (denoted as  $\epsilon$  in this paper) and  $\epsilon''$  is the dielectric loss. The dielectric loss tangent

( $\tan \delta$ ) is defined as

$$\tan \delta \equiv \frac{\varepsilon''}{\varepsilon'}. \quad (3)$$

The dielectric loss tangent ( $\tan \delta$ ) value of 0.02 of the resulting Fe@SiO<sub>2</sub>/polymer nanocomposites means that only 2% of charges induced by the external field were dissipated. This results indicates that the SiO<sub>2</sub> protection layers and PDMS matrices are effective ways to isolate the iron nanoparticles and prevent them from conducting charges, thus leading to polymer composites with low dielectric loss ( $\tan \delta$ ).

#### 4. Conclusions

We have demonstrated the feasibility of preparing low loss, Fe@SiO<sub>2</sub> nanoparticle polymer composites with improved magneto-dielectric properties at radio frequencies (1 MHz–1 GHz). We have developed a simple method to obtain iron nanoparticles with uniform size distribution by utilizing citric acid and oleic acid as surface-capping agents. The particle size was tailored by tuning the concentration ratio of iron ions to carboxylic acid groups. The Fe nanoparticles were successfully coated by a layer of silica (SiO<sub>2</sub>) to prevent Fe cores from oxidizing. The dielectric permittivity and magnetic permeability of the resulting Fe@SiO<sub>2</sub>/polymer composites increased with higher weight percentage of Fe@SiO<sub>2</sub> nanoparticles. The low dielectric loss of the composites is attributed to the ability of SiO<sub>2</sub> layers and polydimethylsiloxane matrix to hinder the conductive nature of metallic iron.

#### Acknowledgments

This material is based upon work supported by the Air Force Office of Scientific Research, grant no. FA95500910430. We also acknowledge the support of the Maryland NanoCenter and its NispLab. The NispLab is supported in part by the NSF as a MRSEC Shared Experimental Facility.

#### References

- [1] Moulson A J and Herbert J M 2003 *Electroceramics: Materials, Properties, Applications* (West Sussex: Wiley) p 502
- [2] Cullity B D and Graham C D 2009 *Introduction to Magnetic Materials* (Hoboken: Wiley) p 418
- [3] Lebourgeois R, LeFur C, Labeyrie M, Pate M and Ganne J P 1996 *J. Magn. Magn. Mater.* **160** 329
- [4] Huber D L 2005 *Small* **1** 482
- [5] Wu L Z, Ding J, Jiang H B, Chen L F and Ong C K 2005 *J. Magn. Magn. Mater.* **285** 233
- [6] Wu L Z, Ding J, Jiang H B, Neo C P, Chen L F and Ong C K 2006 *J. Appl. Phys.* **99** 083905
- [7] Farrell D, Majetich S A and Wilcoxon J P 2003 *J. Phys. Chem. B* **107** 11022
- [8] Dumestre F, Chaudret B, Amiens C, Renaud P and Fejes P 2004 *Science* **303** 821
- [9] Peng S, Wang C, Xie J and Sun S 2006 *J. Am. Chem. Soc.* **128** 10676
- [10] Ling T et al 2009 *Nano Lett.* **9** 1572
- [11] Wang S, Cao H, Gua F, Li C and Huang G 2008 *J. Alloys Compounds* **457** 560
- [12] Yuan M I, Tao J H, Yan G J, Tan M Y and Qiu G Z 2010 *Trans. Nonferrous Met. Soc. China* **20** 632
- [13] Wen J Y and Wilkes G L 1996 *Chem. Mater.* **8** 1667
- [14] Kobayashi Y, Horie M, Konno M, Rodriguez-Gonzalez B and Liz-Marzan L M 2003 *J. Phys. Chem. B* **107** 7420
- [15] Zhang Z, Zhou F and Lavernia E J 2003 *Metall. Mater. Trans. A* **34** 1349
- [16] Enustun B V and Turkevich J 1963 *J. Am. Chem. Soc.* **85** 3317
- [17] Turkevich J and Kim G 1970 *Science* **169** 873
- [18] Henglein A and Giersig M 1999 *J. Phys. Chem. B* **103** 9533
- [19] Toneguzzo P, Viau G, Acher O, Fievet-Vincent F and Fievet F 1998 *Adv. Mater.* **10** 1032
- [20] Pierre J L and Gautier-Luneau I 2000 *Biomaterials* **13** 91
- [21] Willard M A, Kurihara L K, Carpenter E E, Calvin S and Harris V G 2004 *Int. Mater. Rev.* **49** 125
- [22] Wu N Q, Fu L, Su M, Aslam M, Wong K C and Dravid V P 2004 *Nano Lett.* **4** 383
- [23] Wagner C D 1991 *The NIST X-ray Photoelectron Spectroscopy (XPS) Database* (Gaithersburg, MD: Dept. of Commerce, National Institute of Standards and Technology)
- [24] Salgueirino-Maceira V, Correa-Duarte M A, Hucht A and Farle M 2006 *J. Magn. Magn. Mater.* **303** 163
- [25] Grzelczak M, Perez-Juste J, Rodriguez-Gonzalez B, Spasova M, Barsukov I, Farle M and Liz-Marzan L M 2008 *Chem. Mater.* **20** 5399
- [26] Duran A, Serna C, Fornes V and Fernandez Navarro J M 1986 *J. Non-Cryst. Solids* **82** 69
- [27] International Centre for Diffraction Data 1991 Powder diffraction file alphabetical index (Swarthmore, Pa, USA) *US Patent Specification* 06-0696
- [28] Yang T I, Brown R N C, Kempel L C and Kofinas P 2008 *J. Magn. Magn. Mater.* **320** 2714
- [29] Yang T I, Brown R N C and Kofinas P 2009 Effect of particle domain wall movement and characteristic length on the radio frequency magnetodielectric properties of polymer composites *ACS PMSE Proc.* Washington, DC
- [30] Dunlop D J 1981 *Phys. Earth Planet. Inter.* **26** 1